Available at: https://doi.org/10.1002/admt.202000910

Printed Iontophoretic-Integrated Wearable Microfluidic Sweat-Sensing Patch for On-Demand Point-Of-Care Sweat Analysis

Brince Paul, Silvia Demuru, Céline Lafaye, Mathieu Saubade, Danick Briand **

Dr. B. Paul, S. Demuru, Dr. D. Briand
Soft Transducers Laboratory (LMTS)
École Polytechnique Fédérale de Lausanne (EPFL)
2000 Neuchatel, Switzerland
E-mail: brince.paulkunnel@epfl.ch; danick.briand@epfl.ch

Dr. C. Lafaye, Dr. med M. Saubade
Sports Medicine Unit, Swiss Olympic Medical Center
Division of Physical Medicine and Rehabilitation
Centre hospitalier universitaire vaudois (CHUV)
1011 Lausanne, Switzerland

Keywords: on-demand sweat analysis, capillary effect, multisensing sensor array, printed iontophoretic, wearable point of care

In recent years, wearable epidermal sweat sensors have received extensive attention owing to their great potential to provide personalized information on the health status of individuals at the molecular level. For on-demand medical analysis of sweat in sedentary conditions, a cost-effective wearable integrated platform combining sweat stimulation, sampling, transport, and analysis is highly desirable. In this work, a printed iontophoretic system integrated into a microfluidic sensing platform, which combines sweat induction, collection, and real-time analysis of sweat-ions into a single patch for on-demand sweat monitoring on human subjects in stationary conditions is reported. The incorporation of microfluidics features facilitates sweat sampling, collection, and guiding through capillary effect. The multi-sensing sensor array exhibits sensitivity close to Nernstian behaviour for sodium, potassium, and pH. The correlation between the concentrations of ions measured with the sweat patch and with ion chromatography analysis demonstrates the applicability of the system for real-time point-of-care monitoring of the health status of individuals. Furthermore, the sweat patch electronic interface with wireless transmission enables real-time data monitoring and storage over a cloud platform. This printed

iontophoretic-integrated fluidic sweat patch provides a cost-effective solution for the on-demand analysis of sweat components for healthcare applications.

1. Introduction

Wearable sensors and electronics have garnered great attention in personalized healthcare and fitness monitoring owing to their inherent advantages such as lightweight, flexibility, conformability, miniaturization, and ability to replace bulk and complex measurement systems, enabling notably real-time monitoring.[1] Recent advances in wearable technology have opened up great promises in wireless electrophysiological parameters monitoring, including electroencephalography (EEG), electrocardiography (ECG), electromyography (EMG),[2-8] and more recently in the monitoring of analytes within body fluids.[9,10] Integration of advanced flexible and soft materials and novel fabrication technologies have facilitated the development of skin interfaced devices performing molecular level detection from tears, sweat, and interstitial fluid.[11] The intelligent design and conformal attachment of these technologies on the human body have enabled an accurate collection of these biofluids and multiplexed analysis of biochemical analytes present in them, which could provide relevant information on the dynamic health status of individuals.[1, 12] Recently, several research groups are trying to establish strong correlations between the concentration of the biochemical analytes present in body fluids and blood.[13-16] The imminent capability of wearables for the effective non-invasive sampling and analysis of biofluids and their accurate correlation with blood analytes is representing a very promising alternative solution to blood analysis for point-of-care diagnostics.

Among the various biofluids, sweat, which contains biologically relevant markers such as ions, heavy metals, metabolites, and proteins, was of growing interest in healthcare monitoring and disease diagnostics.[11,17] The sweat excreted by eccrine sweat glands, contains many clinically pertinent ions, and the markers diffused from the bloodstream reflect health status at a chemical

level.[13,18,19] For example, the concentration of sodium in sweat could be used as a marker for electrolyte imbalance and the measurement of the dehydration status of the body. [20] Similarly, chloride levels in sweat are useful for screening cystic fibrosis,[21] potassium level correlated with plasma for ambulatory monitoring and sweat quality control , [22, 23] pH as an indicator of metabolic alkalosis, [24] glucose for screening prediabetic conditions[25] or monitoring tool for diabetes,[23] and lactate for assessing metabolic efficiency.[26] Interestingly, several works have shown that lactate levels and ethanol levels in sweat have a strong correlation with corresponding blood concentrations.[27-29] However, classical sweat evaluations need many equipment and skills, limiting research in this area. Therefore, sweat represents a relevant biofluid for continuous non-invasive monitoring of physiological health status or in clinical conditions, and thus a wearable epidermal device that facilitates sweat sampling, collection, transport, and analysis is extremely desirable. Making such a non-invasive tool available could revolutionize healthcare, and accelerating medical research to progress in this field.

Multiple research groups have conducted extensive effort to develop epidermal wearable devices for real-time sweat monitoring based on different transduction mechanisms such as field-effect transistors, electrochemical, and colorimetric methods. Zhang *et al*. demonstrated complementary metal-oxide-semiconductor (CMOS) ion-sensitive field-effect transistors (ISFETs)-based wearable system for multiple ion sensing from sweat, with sensitivities close to the Nernstian limit.[30] Javey *et al.* produced an electrochemical-based wearable system on a flexible polyethylene terephthalate (PET) substrate by photolithographic processes for monitoring ions and metabolites from sweat.[31] For an enhanced interface with the skin, Wang *et al.* developed tattoo based epidermal wearable sensors for monitoring sweat electrolytes and metabolites.[32,33] A shift towards printed and laser patterned electrodes on flexible platforms for standard electrochemical-based and transistors-based sensors, enabled cost-effective high-throughput fabrication by eliminating the requirement of multistep photolithographic and

etching processes.[34-36] Integration of microfluidics with a sensor array facilitated sweat capture, store, and consistent analysis at lower sweat volume.[37-38] Based on this, Rogers *et al*. established optical-based skin mountable wearable systems for colorimetric analysis of various biomarkers and ions from the sweat.[39]

Natural methods of sweat induction can lead to uncontrolled sweat generation at different locations.[40] Although exercise is a common method for sweat induction that can be easily applied to athletes and amateur sportsmen, an alternative way of sweat stimulation is required for on-demand sweat analysis. The latter would be particularly valuable to gather information on the health status of sedentary individuals or for medical analysis in sedentary conditions.[1,41] The sweat induction in humid and hot conditions such as, Sauna or bathing is not practical and user-friendly for sweat collection. Moreover, An active and controlled sweat induction enables temporal sweat analysis at different locations on the body and is more appropriate for point-of-care applications.[36] To address this challenge, iontophoresis, a chemically-induced localized secretion of sweat, has been developed, and it is commercially available as a bulky wearable system.[42] Recent studies on local sweat induction by an iontophoretic method, as well as commercially available sweat analysis devices, require separate procedures for sweat stimulation and collection.[36] A demonstration on blood-correlated sweat sensing device for ethanol uses external commercially available sensors.[43] Some progressive efforts have been made to use iontophoresis in combination with sweat sensing platforms. A tattoo-based sensor for on-body alcohol monitoring,[44] an autonomous platform for cystic fibrosis monitoring,[45] epidermal enzymatic sensor for monitoring vitamin C level[46]. However, some of them are not fully integrated, involve inconvenient and costly cleanroom fabrication processes, or lack some functionalities, such as microfluidics for continuous sweat sampling. The latter leads to the exposure of the sensing surfaces directly on the skin, thereby resulting in sensor contamination and mixing of sweat over time. Interestingly, Lee et al. reported an integrated wearable patch for monitoring of diabetes and feedback drug delivery.[13] But, this closed-loop system lacks

the sweat induction module and the fluidics module for sweat collection. The recent work of a smartwatch has demonstrated an integrated platform for glucose monitoring.[47] However, this system utilized cleanroom fabrication techniques such as e-beam evaporation for electrode array fabrication. Further, the device utilized a ring-shaped hydrogel surrounding the entire microfluidic patch for the stimulation, which could suffer efficient sweat sampling at the inlet as induced sweat needs to flow into the inlet of the device. To address these limitations, we have developed a cost-effective printed electronic-based iontophoretic device integrated with microfluidics and sensing functionalities in a single patch, which facilitates sweat induction encircling the inlet of the fluidic patch and fast uptake of sweat through the capillary tube provided at the inlet of the patch as soon as sweat excretion begins.

Herein, we report on a printed iontophoretic integrated fluidic sweat patch (IIFSP) for on-demand sweat analysis on subjects in stationary conditions. The sweat ion-selective sensor arrays, and iontophoretic electrodes with the agonist agent for sweat stimulation, were fabricated via screen printing on a flexible PET substrate. The microfluidic architecture, which enables sweat sampling, collection, and transport, was devised in PET using laser patterning and integrated to the sensors and iontophoretic layers by vertical stacking of patterned adhesive layers, to obtain the 3D architecture of the final sweat patch. The microfluidic incorporation prevents the sensing electrodes from being in direct contact with the skin, avoids the contamination of the sensing layer from the direct agonist agent exposure, and diminishes the sweat volume necessary for analysis. In comparison to the cleanroom processes, the high throughput fabrication by printing and laser patterning enables the realization of the cost-effective manufacturing of the IIFSP. In addition, it enables the reusability of the electronics readout, microfluidics, and iontophoresis stimulation electrodes. The IIFSP system facilities sweat stimulation, collection, and simultaneous monitoring of sodium, potassium, and pH ions concentrations from human sweat. The characterization of the sensing capability of the fabricated sensor patches was performed in the respective ion solutions and artificial sweat for

sensitivity analysis. Real-time on-demand demonstration of iontophoresis and sensing was performed on human subjects and the sweat ions concentration data was displayed on a smartphone wirelessly using a custom build android app. Also, the measured data were correlated with ion chromatography analysis which is considered as a reference method for sweat analysis.[48] Thus, the cost-effective manufacturing of the IIFSP and the successful demonstration of its capability for real-time sweat analysis pave the way for the time-dependent monitoring of sweat components, for personalized health status and point of care medical analysis of individuals.

2. Results and Discussion

2.1. Overall design of the IIFSP and interface

The overall principle of IIFSP patch operation includes iontophoretic stimulation for sweat induction, sampling, and transport of induced sweat by microfluidics, and finally the analysis of the sweat ionic content by the sensors array integrated into the microfluidics reservoir. The total size of the IIFSP patch (length: 6 cm and width: 3.5 cm) is designed by conceiving many factors such as the minimum required sweat induction area (1 cm^2) for an adequate sweat sampling in a limited time, areal consideration of the ion-selective sensors for better signal transduction, geometrical necessities of the microfluidics (central length: 16.4 mm, central width: 3.5 mm) for a passive constant sweat flow by avoiding any evaporation while having an appropriate placement of the sensor array without causing hindrance during the sweat flow, and a better attachment to the human skin and circuit interface. **Figure 1**a illustrates the iontophoretic-integrated fluidic sweat patch (IIFSP) mounted on a subject's wrist for sweat analysis. As shown in the exploded view of the sweat patch, the sweat patch consists of three main modules: sweat stimulation module, sweat transport module, and sweat sensing module, all fabricated on a PET substrate using printing processes. The vertical integration of these three

modules in a 3D manner results in the final sweat patch, including sweat induction, sweat carriage, and sweat components analysis in a single epidermal wearable device. The key features that we considered for the realization of the IIF sweat patch include the cost-effectiveness of the materials and processes, the user-friendliness for handling and printing, stability with low strain in data acquisition, and eases in electronic interfacing.

A medical-grade adhesive layer is used to attach the patch to the skin, which enables the tight seal to the skin and avoids mechanically-persuaded irritation on the underline skin. The engineered design of the IIF sweat patch sensor array eases its interfacing to readout electronics. The sweat stimulation module incorporates a pair of electrodes, called respectively stimulation and return electrode, fabricated on a PET substrate to induce the generation of sweat by applying a small current across the electrode using the iontophoretic approach. These stimulation electrodes are coupled with a cholinergic agonist agent, pilocarpine, loaded in hydrogels using a polymethyl methacrylate-based gel holder, which provides a stable skin interface. The coverage of the hydrogels prevents the direct contact of the electrodes with the epidermal surface, and therefore the occurrence of skin burning. During the iontophoresis process, a small current applied at the stimulation electrode delivers the cholinergic agent across the skin, which binds to the acetylcholine receptors of the sweat glands to induce the sweat. Figure 1b illustrates the sweat induction by the iontophoretic process compared with the natural sweating phenomena. The induced sweat is swiftly drifted to the transport module through the capillary tube at the inlet of the patch.

The sweat transport module contains microfluidic features that are laser patterned into a PET substrate. The implementation of the microfluidics facilitates (i) protection of sensor array electrodes against contamination by avoiding their direct contact with the skin, and (ii) prevents sensor false reading due to evaporation of sweat. The microfluidic features include a 1 mm in diameter inlet matching with the inlet of the iontophoretic module, a fluidic channel (150 µm wide) that connects to a detection chamber (3.5 mm wide at its center), and an outlet (2 mm in

diameter) that eliminates backpressure in the fluid flow. The microfluidic architecture was engineered to obtain the fast uptake of sweat as soon as its excretion begins, and to drive quickly the sweat to the detection chamber until the maximum fluid intake capacity (approximately 12 µL) of the microfluidic features is reached. Furthermore, the sweat transport module enables continuous replacement of old accumulated sweat from the chamber, owing to the natural osmotic pressure of the secreted sweat and the capillary action at the inlet. As sweat fills in the detection chamber, the sensor array located within that chamber reads the ion concentrations in the collected sweat.

The IIFSP sensing module consists of an electrochemical electrode array patterned on a PET substrate by screen printing (the fabrication process is detailed in the Experimental section). The sensor array comprises three carbon-based ion-selective working electrodes (1.5 mm in diameter) and a shared Ag/AgCl based common reference electrode (1 mm × 1.5 mm area) for the analysis of Na^+, K^+, and pH ions present in sweat. A sodium ionophore X-based membrane is used on one of the ion-selective electrode (ISE) for the selective detection of Na^+, whereas K^+ ion detection is accomplished by using an ISE coated with a valinomycin-based membrane. Polyaniline (PANI)-electrodeposited ISE serves as a pH sensor for the detection of H^+ by a deprotonation process.[49] The Ag/AgCl reference electrode is coupled with a polyvinyl butyral (PVB) membrane, which enables to maintain a stable reference potential in solutions with different ionic strength.[52] The chloride added to the PVB membrane prevents direct Cl^- ions interaction with the Ag/AgCl reference electrode and thus minimizing the voltage drift. The potential of the respective ISEs corresponding to Na^+, K^+, and H^+ ions concentration was detected with respect to the stable reference electrode.

A two-layer printed circuit board (PCB) is developed to interface the IIFSP, which includes signal conditioning, processing circuits, and wireless transmission module for on-body sweat analysis. By considering the cost-effective manufacturing and high throughput strain-free data transmission, a rigid PCB having a footprint size of 6 mm length X 5 mm width is selected to

accommodate the electronics (size that enables the manual placing and soldering of electronic components), the battery, and a suitable attachment on the human arm. Efficient power management is implemented by avoiding the simultaneous operation of iontophoresis and sensing modes, which minimizes the large power consumption. The iontophoretic process required 1.3 mA, and the sensing module was implemented by low power AD 8608 (operating current: 1mA, Analog Devices) based amplifier and low power SAMD 21 based MCU (1.62V minimum operating voltage). In view of the long duration of operation and multiple subject analysis, a lithium-ion polymer battery on the order of 1200 mAh capacity is selected for powering the system. The data transmission over WIFI facilities stable data fidelity and remote monitoring. However, a miniaturized battery with a capacity of 500 mAh would be adequate for short duration analysis applications. Figure 1c shows the block diagram of the developed PCB. The analog circuits, including the individual high impedance voltage buffers for the signal acquisition of the Na^+, K^+, and H^+ sensors, the bias circuit for reference voltage, and low pass filters for stable output voltage, are designed and interfaced with a microcontroller (MCU) module. The MCU module integrates a 12-bit analog to digital converter (ADC), which was used to convert the analog signals to digital signals, and its transmission by using the on-chip WIFI module. The iontophoretic-circuit module, which consists of a DC-DC converter, voltage to current converter for the current setting, and a switch for the stimulation control, was coupled to the main PCB. A single rechargeable lithium-ion battery (3.7 V) was used to power the PCB. A custom-built open-source application was developed to display and share the IIFSP results on a smartphone. The system interface also facilitates data upload on a custom-developed cloud server, which could be retrieved for future analysis.

2.2. In vitro characterization of sensors

The characterization of H^+, K^+, and Na^+ sensors was performed *in vitro* in their respective electrolyte with physiologically relevant ion concentrations. **Figure 2**a shows the open circuit potential (OCP) response of the H^+ sensor tested in McIlvaine buffer solutions with its pH varying from 4 to 8. The stable output voltage response of the pH sensor shows that the electrodeposited PANI is highly sensitive to H^+. The sensitivity of the pH sensor was found to be 61.1 mV/decade of ion concentration, exhibiting a nearly-Nernstian behavior (Figure 2(d)). Similarly, the performance of the K^+ and Na^+ sensors were evaluated in electrolyte solutions with concentrations of 1-32 mM K^+ and 1-160 mM Na^+, respectively (Figure 2b,c). Both sensors exhibited fast responses with near-Nerstian behavior sensitivities of 66.2 mV/decade and 64.8 mV/decade of respective ion concentration (Figure 2e, f). Figure S1 (Supporting Information) depicts the stability analysis of the PVB-coated Ag/AgCl reference electrode. A maximum potential drift of 3 mV over a 2 hours period reveals that the developed reference electrode can maintain a stable voltage during continuous measurement with the potentiometric sensors.

To investigate the repeatability of the developed sensors, the dynamic response of H^+, K^+, and Na^+ ion-selective sensors were performed under the successive changes of the concentration of the electrolyte from low to high and then high to low in one and a half cycle. **Figure 3**a shows the response of the H^+ sensor in the buffer solutions of varying pH. H^+ sensor exhibited a near-Nernstian reaction with an average sensitivity of 62.3 mV/decade in one and half-cycle repeated measurements. The fast response with a small 0.79% relative standard deviation (RSD) of its sensitivity indicates the good reversibility and repeatability of the fabricated pH sensor. K^+ sensor exhibited an average sensitivity of 66.0 mV/decade with 1.36% RSD, whereas Na^+ showed an average sensitivity of 65.2 mV/decade with 1.22% RSD in one and half-cycle repetitive testing (Figure 3b,c). This result indicates that the K^+ and Na^+ sensor responses are

recoverable. To assess the reproducibility of the fabricated sensors, five of each of the H^+, K^+, and Na^+ sensors were tested in their respective standard electrolyte solutions with varying 4-8 pH, 2-32 mM K^+, and 10-160 mM Na^+ concentrations, respectively. As presented in Figure S2 (Supporting Information), the H^+, K^+, and Na^+ sensors exhibited good reproducibility with an average sensitivity of 62.5 mV/decade (2.3% RSD), 65.5 mV/decade (4.2% RSD), and 64.4 mV/decade (4.3%RSD), respectively. However, the fabricated sensors experienced changes in their absolute potential in the same respective concentration of analytes. The variations of the absolute potential values of sensors, which arise due to some variability in the preparation and the drop-casting processes, can be resolved by two-point calibration and baseline correction (Figure S3, Supporting Information).

The ability to selectively detect the target ion among the interfering substances is the one main requirement during the development of ion-selective sensors for sweat analysis. **Figure 4**a-c depicts the selectivity evaluation of H^+, K^+, and Na^+ sensors, respectively, in the presence of possible interfering ions at physiologically relevant concentrations. It was observed that the response of the sensors due to the interfering ions was significantly less than the response for the respective target ions, which implies that the ion-selective sensors have a specific response. In addition, the interference due to the pilocarpine, the agonist agent used in the iontophoretic process, is negligible (Figure S4, Supporting Information). Finally, the temperature has a negligible influence on the response of the potentiometric sensors (Figure S5, Supporting Information). Besides, the ion-selective sensors' responses exhibited negligible variation in sensitivities over four weeks (stored at 4 °C), with RSDs of 2.52% for H^+, 2.45% for K^+, and 2.5% for Na^+ (Figure S6, Supporting Information).

2.3. Microfluidic design, integration, artificial sweat testing, and on-body characterization

The microfluidic architecture was designed by considering different factors such as adequate sweat collection, high sweat flow rate, minimal sweat evaporation, and minimal back pressure sources for an unhindered sweat flow (Figure S7, Supporting Information). One constraint to the optimization of the geometrical parameters of the microfluidic features was the channel height defined by the spacer layer, which includes the PET and adhesive layers thicknesses used for the fabrication of the channel. The other geometrical parameters were optimized analytically by applying the Poiseuille's law, which accounts for the flow rate dependency on the length and width of the different sections of the microfluidic structure, as depicted in **Figure 5**a,b.[51] As shown, the flow rate of the structure was directly proportional to the width, whereas inversely proportional to the length of the structures. A minimum length of 3.5 mm was selected for the inlet channel for enhanced sweat sampling while maintaining a sufficient flow rate. It was also observed that the pressure drop decreases when the width of the channel increases (Figure 5c). Thus, a channel width of 150 µm was chosen to avoid larger pressure drops, since channels with larger width (>200 µm) might induce sweat evaporation.[37] The geometrical dimensions of the reservoir were constrained by the area of the enclosed sensor array, with its central width and its length set at 3.5 mm and 16.4 mm, respectively. These dimensions enabled the appropriate placement of the sensor array without causing any hindrance to the sweat flow while providing minimal dead volume and filling time. The channel length of the outlet was designed to relieve the backpressure, allowing unimpeded sweat flow. As backpressure linearly varies with the channel length of the outlet (Figure S8, Supporting Information), a small channel length of 0.6 mm was selected to diminish the effect of the backpressure. The sweat flow profile in the designed microfluidic structure was evaluated by drop-casting a color dye into the inlet sensor array. Figure S9 (Supporting Information) displays the progress of the dye secretion

without any leakage, which validated the robustness of the material and architecture used for sweat sampling and transport.

To further characterize the sensor array while implemented into the fluidic channel, its chemical responses were evaluated in artificial sweat at a constant flow rate using a commercial syringe pump. By considering that the arm region contains 150 glands/cm^2 with an average flow rate of 10 nL/min/gland, a maximum constant flow rate of 2 µL/min was maintained during the measurements, considering that sweat coming from a stimulated area of 1 cm^2 could flow into the inlet.[17] Figure 5d-f depicts the OCP responses of pH, K^+, and Na^+ sensors, respectively, in the artificial sweat (2 µL/min flow rate) with varying concentrations of the corresponding ions within physically relevant ranges. The sensors exhibited a near-Nernstian behaviour and the sensitivities obtained in artificial sweat are nearly equal to those obtained in the standard electrolyte solutions (Figure 5g-i). The variations observed in the absolute potential values can be adjusted by calibration and by baseline correction. This study demonstrated the successful response of the sensor array after microfluidic integration and in complex fluids such as artificial sweat.

To characterize the stability of the IIFSP interface to the electronic module, the interconnection resistance of ion-selective sensors connectors was measured (Figure S10, Supporting Information). All three ion-selective sensors exhibited an interconnection resistance of less than 0.3Ω, demonstrating the printed connectors' efficiency for an electronic interface. Further, a less than 3% change in the ion-selective sensors' resistance and their interconnection resistance during bending state indicates the robustness of IIFSP towards the mechanical deformations (Figure S11a,b, Supporting Information). This minimal change in resistance is attributed to the printed PU insulating layer, which protects the conductor against high stress build-up during slight bending states. Besides, the IIFSP demonstrated minimal changes (<5%) to

interconnection resistance before and after daily events (Figure S12, Supporting Information). In addition, to investigate the stability of the signal during skin interface, with an IIFSP well-fixed to the wrist of the subject and filled with artificial sweat, the sensors' responses were recorded when the subject was undergoing various arm motions such as wrist rotation, arm-waving, and arm vibration (Figure S13a,b,c Supporting Information). A negligible fluctuation (<10.5% compared to baseline) of IIFSP's sensors responses was observed during all these arm motion conditions. Similarly, IIFSP's sensors responses during the subject's daily routine, including sitting, standing, and slow walking, were recorded, as shown in **Figure 6**. The observed sensor's maximum fluctuations during these activities were less than 9.4% compared to base line. These experimental results indicate the robustness of the developed IIFSP for sweat analysis during sedentary conditions with minimal body motion. These experimental results indicate the robustness of the developed IIFSP for sweat analysis during sedentary conditions with minimal body motion.

2.4. Printed iontophoretic-based sweat stimulation and *in vitro* validation

The performance of the printed iontophoretic-based system was optimized in terms of current intensity and time of the delivery, to get the maximum secretion of sweat. For this optimization, standard Pilogels (ELITech group) were used in the printed electrodes, coupled with custom-made PMMA gel holders, and placed on the skin (Figure S14a, Supporting Information). Current profiles with different intensities and duration were applied across the iontophoretic electrodes. The secretion of sweat occurred after a few minutes of the iontophoresis process. It was observed that a higher current intensity profile, with a longer duration of stimulation, induced a higher quantity of sweat. However, by considering efficient sweat induction without provoking skin irritation, the stimulation current was fixed at 1.3 mA for a duration of 10 min. The capability of the printed electrodes array for sweat stimulation was validated by comparing

it with a standard sweat stimulator (ELITech group). The sweat induced by both stimulators was collected using a standard Macroduct sweat collector (ELITech group), and it was observed a similar flow dynamics (Figure S14b,c, Supporting Information), confirming the efficiency of the printed electrodes for sweat stimulation.

To further evaluate the capability of the microfluidic patch for combined sweat induction and sampling, the patch was placed on the skin, with the iontophoresis process conducted using the optimized parameters, achieving efficient delivery of the stimulating agonist agents to induce the sweat (Figure S15a, Supporting Information). After the iontophoretic process, the sweat began to flow into the microfluidic patch through the capillary channel present at the inlet. The sweat flowed radially from the inlet channel, through the reservoir, to reach the outlet of the patch (Figure S15b, Supporting Information). It was observed that the reservoir was filled in 11 min, and the sweat reached the outlet of the channel in 13 min. Based on the total volume of the sweat patch and the total time taken for its complete filling, the sweat flow rate was experimentally calculated to be 0.92 µL/min. Thus, the sweat rate per gland was assessed to be 6.1 nL/min, assuming that the stimulated sweat that could flow into the inlet was from a 1 cm^2 skin area. Altogether, the stimulation experiments show the capability of the printed iontophoretic-integrated microfluidic device for sweat secretion and collection, comparable to standard commercial systems.

2.5. On-body sweat monitoring using IIFSP

The feasibility of the developed IIFSP for wearable healthcare applications was demonstrated by performing on-body sweat analysis. The sensor array was calibrated by a two-point calibration method before and after the measurement. In order to validate the IIFSP, the concentration profiles of the respective sweat ions from the sensors array were compared with the results obtained from the reliable ion-chromatographic measurements. The consistent

relationship between the ion-selective sensors measurements and ion-chromatographic readings, as shown in **Figure 7**, indicates the potential of the developed sensor array integrated into the patch for ion detection in sweat. To demonstrate the usefulness of the sweat patch for wearable application, the IIFSP was interfaced with the electronics PCB and the combined system was tightly fixed to the forearm of healthy subjects, as shown in **Figure 8**a. The sweat stimulation process was performed by activating the iontophoretic module for a duration of 10 min to induce the sweat. After the iontophoretic process, the sweat secretion was initiated and sweat started to accumulate slowly in the detection chamber of the patch (Figure 8b). The data readout from the sensor array started approximately 4 min after the perspiration occurred. Thus, the IIFSP sensor module was activated after 10 min of iontophoresis stimulation and 4 min of accumulation period. As sweat takes some time to fill the detection chamber of the patch, and thus to interact with the sensors, until which only the background signals of the sensors were recorded. An abrupt change in sensor response occurred as soon as the detection chamber was filled with sweat, and reached a stable value after a few minutes, once a steady flow of sweat was established (Figure S16, Supporting Information). The IIFSP readings were wirelessly transmitted and displayed in real-time on the smartphone-based application (Figure S17, Supporting Information).

Figure 8c shows the profiles of ion concentrations in sweat from three subjects, measured using the IIFSP. For all, the readings of the respective ion sensors exhibited initial fluctuations when the sweat began to fill the chamber, as the sweat takes some time to properly interact with the sensors. The sensors' readings were stabilized after several minutes of sufficient sweat sampling and the steady flow of sweat occurred. The stable responses of the sensors were considered for estimating the sweat analyte concentrations. It was observed that the response time of the sensor array varied among the subjects because of the different sweat secretion process depending on the individual. However, ion-selective sensors reading followed a similar

trend for all the subjects. The results highlight the efficiency and effectiveness of the fabricated iontophoretic-integrated microfluidic sweat patch for sweat induction, sampling, and analysis of the concentrations of ions in sweat. To further demonstrate the capability of the IIFSP to monitor rate dependence of sweat ions concentrations, the IIFSP sensors readings were recorded by varying the applied iontophoretic duration, which modulates the sweat secretion rate on a subject. The ion-selective sensors' initial sweat interaction readings (before the sensor's responses saturate) were considered for establishing the sweat rate relationship. The corresponding approximate sweat flow rate was calculated based on the total volume of sweat patch and the sweat's total time to reach the outlet. It was observed that concentrations of Na^+ and K^+ ions mainly increasing with sweat rate, whereas the H^+ sensor showed a slight increment with sweat rate compared to Na^+ and K^+ ions (Figure S19, Supporting Information). A similar trend of increasing the Na^+ and K^+ ion concentrations with the increase in sweat rate was previously reported for sweat produced during exercise conditions. [17, 36] Here, the different sweat secretion rate is achieved by a different iontophoresis stimulation duration. The proportional relationship of sweat rate and ionic concentration profile provides an effective way of maintaining electrolyte balance in individuals for physiological health status. The accurate measurement of the sweat rate is possible by implementing electrodes and admittance measurements corresponding to sweat flow.[59] These studies demonstrate the strong potential of the IIFSP for sweat analysis during stationary conditions in healthcare applications. Compared to some already reported ion-selective sensors for sweat sensing applications that are either not iontophoretic integrated or microfluidic incorporated, IIFSP shows a breakthrough by combining printing, sweat stimulation, microfluidics, and analysis functionalities in a single practical wearable platform (Table S1, Supporting Information). The Field-Effect Transistor (FET)-based ion-sensitive sensors such as ISFETs offer lower drift and easier miniaturization, and so the possibility of integration with multiple sensor arrays with lower sweat volume necessary for analysis.[30] However, the requirement of the dedicated

cleanroom fabrication facilities, higher manufacturing cost, and more complex electronics for the integration are the critical limitations of the ISFET technology as compared to the OCP-based transduction devices. Using high-resolution screen printing and digital printing technologies such as an inkjet or aerosol jet, we envisage this IIFSP could be further scaled down to incorporate a higher number of sensors for multi analyte sensing through the customization of the system towards a variety of point of care analysis applications, which gathers more attraction than standard MEMS-based miniaturized fabrication technologies, where cleanroom facilities with multistep lithographic and deposition processes are required.

3. Conclusion

We have demonstrated a fully integrated wearable sweat-analysis patch, combining a printed iontophoretic device with a microfluidic multi-sensing platform, for on-demand monitoring of sweat ions such as sodium, potassium, and pH in stationary conditions. The fabricated IIFSP facilitates sweat induction, sweat carriage, and sweat components analysis in a single epidermal wearable device. The incorporation of the fluidic system provides efficient sweat sampling, collection, and transport. The printed electrochemical sensor array showed ions detection from sweat with nearly Nernstian behaviour. Moreover, the correlation of the sweat ions concentrations derived from the system with standard spectroscopy analysis has confirmed the capability of the IIFSP for real-time sweat analysis. On-demand sweat remote monitoring with wireless data recording was validated on three human subjects. Thus, the cost-effective realization of a fully-integrated iontophoretic system and its successful demonstration for sweat induction, collection, and analysis is flagging the way for on-demand analysis of sweat on a variety of individuals, with several future healthcare applications. Notably, on-demand sweat

monitoring at stationary, and its potential correlation to blood analytes, is a promising solution to non-invasive point-of-care monitoring and diagnostics.

4. Experimental Section

Materials: Sodium ionophore X, aniline, potassium ionophore I, bis(2-ethylehexyl) sebacate (DOS), sodium tetrakis[3,5-bis(trifluoromethyl)phenyl] borate (Na-TFPB), cyclohexanone, sodium tetraphenylborate (NaTPB), polyvinyl chloride (PVC), agarose, tetrahydrofuran, BUTVAR B-98 (PVB), pilocarpine, poly(ethylene glycol)-block-poly(propylene glycol)-block-poly(ethylene glycol) (F127), sodium chloride (NaCl), potassium chloride(KCl), citric acid, disodium hydrogen phosphate (Na_2HPO_4), and hydrochloric acid (HCl) were procured from Sigma Aldrich. Silver/silver chloride (Ag/AgCl) ink was purchased from DuPont, whereas carbon paste was obtained from Sun Chemical. All chemical products aforementioned were used without any further purification.

Fabrication of electrode array: The electrodes array for ISE, reference, and iontophoresis was fabricated using a screen-printing process on a 125 µm-thick PET substrate. The stencil for each electrode layer was laser-patterned in PET foil. For the fabrication of the sensor array, first, a reference electrode and conductive lines for the current collectors were printed using the Ag/AgCl ink. Then, respective ISE electrodes for pH, K^+, Na^+ ions were printed using the carbon paste. After their drying at 80° C for 20 mins, the polyurethane (PU)-based encapsulation layer was printed on top and cured at 80° C for 1 h. Similarly, the electrodes for iontophoresis were printed on a PET substrate using Ag/AgCl ink and encapsulated with the PU coating.

Preparation of pH, Na^+, K^+ selective sensors: K^+ ISE membrane was prepared by dissolving 5.142 mM potassium ionophore, 4.174 mM NaTPB, 433.25 mM DOS, and PVC (9.371 wt/vol%) in cyclohexanone. The prepared K^+ mixture was thoroughly mixed for 1 hour to get

the homogenous membrane solution. For Na^+ ISE membrane preparation, 1.5 mM sodium ionophore X, 0.940 mM Na-TFPB, 232.420 mM DOS, and PVC (5 wt/vol%) were dissolved in tetrahydrofuran by thorough mixing until getting the transparent membrane solution. The reference membrane was prepared by dissolving 79.1 mg PVB, 50 mg NaCl, and 2 mg F127 in 1 mL methanol using an ultrasonic bath to get a homogenous mixture of membrane solution. All the prepared ISE membrane solutions were tightly sealed and stored at 4 °C until further use. H^+ ion-selective sensor was fabricated by polymerizing and electrodepositing polyaniline on corresponding H^+ ISE in 0.1 M aniline/1 M HCl electrolyte using cyclic voltammetry with potential from −0.2 to 1 V for 25 cycles at 0.1 V/s scan rate (vs. commercial Ag/AgCl electrode). After 12 cycles of electro-polymerization, the electrolyte solution was replaced with a fresh electrolyte for performing the next 13 polymerization cycles. K^+ and Na^+ ion-selective sensors were fabricated by drop-casting 2 µL of K^+, and Na^+ membrane solutions, respectively, onto their corresponding ISE. The reference electrode was fabricated by drop-casting 5 µL reference membrane solutions onto the Ag/AgCl reference electrode. The modified electrodes were left to dry at 4 °C. The fabricated ISEs were preconditioned with 0.01 M KCl and 0.1 M NaCl for 1 h before the measurements. However, the fabricated ISE could be used without this step for the measurements resulting in a small potential drift (3mV/hr).

Fabrication of microfluidics and IIFSP: The optimized microfluidic features, including inlet channel, reservoir, and outlet channel, were patterned within a thin PET substrate of thickness 125 µm by laser cutting. The via to the inlet channel of the microfluidic feature was created in the PET substrate containing the iontophoretic electrode array, whereas the via from the outlet channel was created in the PET substrate of the sensing electrode array. The gel holding layer of the agonist agents was patterned on a thin PMMA substrate by laser cutting. The 3D construction of the IIFSP was realized by stacking vertically together the gel holding layer, iontophoretic layer, 2D featured microfluidic layer, and sensor array layer using laser patterned double-sided adhesive layers. The capillary tube (1 mm diameter) was embedded and fixed into

the inlet of the channel using an Ecoflex-based adhesive. A biocompatible medical adhesive layer was attached to IIFSP as a skin-interfaceable layer for mounting the patch to the body. For the preparation and incorporation of agonist agent, 3% of agarose gel was prepared by the continuous stirring of agarose in DI water in a glass beaker until a transparent gel was obtained. Then, 1% of pilocarpine was added and vigorously stirred for 1 min. The obtained transparent gel was poured into the gel holding void of the IIFSP and kept at 4 °C for 1 h to solidify the gel.

Sensors characterization and analytes measurement: All the initial characterizations of the ion-selective sensors were executed using the standard commercial electrochemical workstation. For the sensitivity studies of K^+ and Na^+ sensors, KCl (concentration from 2 mM to 32 mM) and NaCl (concentration from 10 mM to 160 mM), respectively in deionized water (DI) was used. For H^+ sensors, Mcllvaine's buffer of pH from 4 to 8 adjusted with Na_2HPO_4 and citric acid concentrations was used. For K^+ and Na^+ sensors selectivity studies, interfering electrolytes such as 1 mM calcium chloride ($CaCl_2$), 1 mM ammonium chloride (NH_4Cl), 100 µM glucose were prepared in DI and successively added to the targeted minimum concentration of electrolytes to be sensed. For H^+ selectivity studies, all interfering electrolytes were prepared in pH 7 solution. The artificial sweat for the K^+ and Na^+ sensors measurements consists of 0.17 mM glucose, 5 mM NH_4Cl, 10 mM urea, and 0.4 mM $CaCl_2$ with varying concentrations of targeted electrolyte.[52] The artificial sweat for the H^+ sensors measurements consists of 6 mM KCl, 50 mM NaCl, 0.17 mM glucose, 5 mM NH_4Cl, 10 mM urea, and 0.4 mM $CaCl_2$ with varying pH. Artificial sweat response measurements were conducted by injecting different concentrations of the targeted analyte solution using a commercial syringe pump at 2 µL/min constant flow rate, and measurements were halted for 30 seconds for each analyte solution change. For agonist agents interfering test, 1% of agonist agent was prepared in a minimum concentration of target electrolyte. The temperature depends on the response of ion-selective sensors that were carried out in the respective electrolytes, in minimum and maximum

concentration levels of the respective ion using separate sensors, with varying temperatures from 25 to 40 °C (with 5 °C increment). Sensors readings were halted until electrolyte temperature reached the targeted temperature for each temperature level. For the mechanical and on-body stability test of the IIFSP, an artificial sweat containing 40 mM Na^+, 8 mM K^+, at pH 6, was used and the inlet and outlet of IIFSP were closed to avoid evaporation. For recording the acceleration during on-body motion analysis, a smartphone having an accelerometer was attached to the subject forearm. The ion chromatography measurement was performed using ProfIC Vario 15 Cation (Metrohm) at room temperature. For the ion chromatographic analysis, the collected sweat samples were initially conserved at 20°C. Before the measurements, the samples were kept at room temperature, and after reaching that temperature, the samples were diluted (1:100 ratio) with 18 MΩ ultrapure water (Milli-Q, Millipore, Billerica).

Circuit design and signal processing: The separate signal conditioning pathways were designed to acquire the signal from H^+, Na^+, and K^+ ion-selective sensors (Figure S20 & S21, Supporting Information). High impedance voltage buffers at each input of the sensors were realized by using the chip AD 8608 (Analog Devices), a low power four-channel amplifier. A low pass filter with a cut-off frequency of about 14.5 Hz was designed at each sensor pathway to eliminate high-frequency noise. The potential to the common PVB reference electrode was fixed by a separate bias circuit with respect to the ISEs, which resulted in positive signals obtained from the ISEs. The processed signals from H^+, Na^+, and K^+ sensors were fed to the ADC of the microcontroller board. A low power SAMD 21 based MCU integrated platform, which possesses a 32KB SRAM memory, a 12bit ADC, incorporated with stand-alone multiride modules (NINA-W10), and easily programmable through Arduino development environment, was used for signal processing and data transmission. The iontophoretic stimulation circuit was realized by combining a DC-DC voltage booster with a V/I converter to deliver a constant current of 1.3 mA. The power delivery to both the sensor module and the iontophoretic module

was achieved by a single 3.7 V lithium-ion battery. An open-source Android-based application was used to visualize the sensor data on the smartphone, where IIFSP wirelessly communicates to the smartphone. The application facilitated the graphical valuation of sensors reading.

***On-body IIFSP sweat analysis procedure*:** On-body evaluation of the developed IIFSP was carried out at EPFL in compliance with the protocol approved by the EPFL Human Research Ethics Committee (HREC No. 057- 2019 / 07.10.2019). Written informed consent was obtained from all the participating subjects. Subjects forehand were wiped with an alcohol swab before attaching IIFSP. The patches were pre-calibrated with a two-point calibration method in a lower and higher concentration of standard electrolyte solution of respective ion sensors before mounting on the body. This calibration enabled the conversion of the acquired ion sensors reading to respective ion concentration after the measurement. For the measurement, first, the iontophoretic module was activated for 10 min to generate sweat. Then, the sensors readings were recorded on the smartphone when the sweat was filling up the sensing patch. Each measurement lasted for 45 min. After the measurement, the patches were post calibrated with a similar method based on two-point calibration to extract accurate reading.

Supporting Information

Supporting Information is available from the Wiley Online Library or from the author.

Conflict of interest

The authors declare no conflict of interest.

Received: ((will be filled in by the editorial staff))
Revised: ((will be filled in by the editorial staff))
Published online: ((will be filled in by the editorial staff))

References

[1] Y. Yang, W. Gao, *Chemical Society Reviews* **2019**, *48*, 1465.

[2] Y. Khan, A. E. Ostfeld, C. M. Lochner, A. Pierre, A. C. Arias, *Advanced Materials* **2016**, *28*, 4373.

[3] A. Chortos, J. Liu, Z. Bao, *Nature materials* **2016**, *15*, 937.

[4] G. Schwartz, B. C.-K. Tee, J. Mei, A. L. Appleton, D. H. Kim, H. Wang, Z. Bao, *Nature communications* **2013**, *4*, 1859.

[5] C. Dagdeviren, Y. Su, P. Joe, R. Yona, Y. Liu, Y.-S. Kim, Y. Huang, A. R. Damadoran, J. Xia, L. W. Martin, *Nature communications* **2014**, *5*, 1.

[6] B. Xu, A. Akhtar, Y. Liu, H. Chen, W. Yeo, S. I. Park, B. Boyce, H. Kim, J. Yu, H. Lai, *Advanced Materials* **2016**, *28*, 4462.

[7] S. Xu, Y. Zhang, L. Jia, K. E. Mathewson, K.-I. Jang, J. Kim, H. Fu, X. Huang, P. Chava, R. Wang, *Science* **2014**, *344*, 70.

[8] D.-H. Kim, N. Lu, R. Ghaffari, Y.-S. Kim, S. P. Lee, L. Xu, J. Wu, R.-H. Kim, J. Song, Z. Liu, *Nature materials* **2011**, *10*, 316.

[9] J. R. Sempionatto, T. Nakagawa, A. Pavinatto, S. T. Mensah, S. Imani, P. Mercier, J. Wang, *Lab on a Chip* **2017**, *17*, 1834..

[10] J. Kim, A. S. Campbell, B. E.-F. de Ávila, J. Wang, *Nature biotechnology* **2019**, *37*, 389.

[11] G. Xu, C. Cheng, Z. Liu, W. Yuan, X. Wu, Y. Lu, S. S. Low, J. Liu, L. Zhu, D. Ji, *Advanced Materials Technologies* **2019**, *4*, 1800658.

[12] J. Choi, D. Kang, S. Han, S. B. Kim, J. A. Rogers, *Advanced healthcare materials* **2017**, *6*, 1601355.

[13] H. Lee, T. K. Choi, Y. B. Lee, H. R. Cho, R. Ghaffari, L. Wang, H. J. Choi, T. D. Chung, N. Lu, T. Hyeon, *Nature nanotechnology* **2016**, *11*, 566.

[14] E. V. Karpova, E. V. Shcherbacheva, A. A. Galushin, D. V. Vokhmyanina, E. E.

Karyakina, A. A. Karyakin, *Analytical chemistry* **2019**, *91*, 3778.

[15] K. McColl, B. Whiting, M. Moore, A. Goldberg, *Clinical Science* **1979**, *56*, 283.

[16] D. A. Dartt, R. R. Hodges, D. Zoukhri, *Advances in organ biology* **2005**, *10*, 21.

[17] H. Y. Y. Nyein, L.-C. Tai, Q. P. Ngo, M. Chao, G. B. Zhang, W. Gao, M. Bariya, J. Bullock, H. Kim, H. M. Fahad, *Acs Sensors* **2018**, *3*, 944.

[18] J. Kim, J. R. Sempionatto, S. Imani, M. C. Hartel, A. Barfidokht, G. Tang, A. S. Campbell, P. P. Mercier, J. Wang, *Advanced Science* **2018**, *5*, 1800880.

[19] J. Choi, Y. Xue, W. Xia, T. R. Ray, J. T. Reeder, A. J. Bandodkar, D. Kang, S. Xu, Y. Huang, J. A. Rogers, *Lab on a Chip* **2017**, *17*, 2572.

[20] A. J. Bandodkar, J. Wang, *Trends in biotechnology* **2014**, *32*, 363.

[21] P. M. Farrell, B. J. Rosenstein, T. B. White, F. J. Accurso, C. Castellani, G. R. Cutting, P. R. Durie, V. A. LeGrys, J. Massie, R. B. Parad, *The Journal of pediatrics* **2008**, *153*, S4.

[22] D. Vairo, L. Bruzzese, M. Marlinge, L. Fuster, N. Adjriou, N. Kipson, P. Brunet, J. Cautela, Y. Jammes, G. Mottola, Scientific reports 2017, 7, 1.

[23] L. B. Baker, Sports Medicine 2017, 47, 111.

[24] M. J. Patterson, S. D. Galloway, M. A. Nimmo, *Acta Physiologica Scandinavica* **2002**, *174*, 41.

[25] J. Moyer, D. Wilson, I. Finkelshtein, B. Wong, R. Potts, *Diabetes technology & therapeutics* **2012**, *14*, 398.

[26] P. Pilardeau, J. Vaysse, M. Garnier, M. Joublin, L. Valeri, *British journal of sports medicine* **1979**, *13*, 118.

[27] D. Sakharov, M. Shkurnikov, M. Y. Vagin, E. Yashina, A. Karyakin, A. Tonevitsky, *Bulletin of experimental biology and medicine* **2010**, *150*, 83.

[28] M. J. Buono, *Experimental physiology* **1999**, *84*, 401.

[29] M. Gamella, S. Campuzano, J. Manso, G. G. de Rivera, F. López-Colino, A. Reviejo, J. Pingarrón, *Analytica chimica acta* **2014**, *806*, 1.

[30] J. Zhang, M. Rupakula, F. Bellando, E. Garcia Cordero, J. Longo, F. Wildhaber, G. Herment, H. Guerin, A. M. Ionescu, *ACS sensors* **2019**, *4*, 2039.

[31] W. Gao, S. Emaminejad, H. Y. Y. Nyein, S. Challa, K. Chen, A. Peck, H. M. Fahad, H. Ota, H. Shiraki, D. Kiriya, *Nature* **2016**, *529*, 509.

[32] W. Jia, A. J. Bandodkar, G. Valdes-Ramirez, J. R. Windmiller, Z. Yang, J. Ramírez, G. Chan, J. Wang, *Analytical chemistry* **2013**, *85*, 6553.

[33] A. J. Bandodkar, W. Jia, C. Yardımcı, X. Wang, J. Ramirez, J. Wang, *Analytical chemistry* **2015**, *87*, 394.

[34] A. E. Ostfeld, I. Deckman, A. M. Gaikwad, C. M. Lochner, A. C. Arias, *Scientific reports* **2015**, *5*, 15959.

[35] Y. Yang, Y. Song, X. Bo, J. Min, O. S. Pak, L. Zhu, M. Wang, J. Tu, A. Kogan, H. Zhang, *Nature Biotechnology* **2020**, *38*, 217.

[36] H. Y. Y. Nyein, M. Bariya, L. Kivimäki, S. Uusitalo, T. S. Liaw, E. Jansson, C. H. Ahn, J. A. Hangasky, J. Zhao, Y. Lin, *Science advances* **2019**, *5*, eaaw9906.

[37] A. Martín, J. Kim, J. F. Kurniawan, J. R. Sempionatto, J. R. Moreto, G. Tang, A. S. Campbell, A. Shin, M. Y. Lee, X. Liu, *ACS sensors* **2017**, *2*, 1860.

[38] J. Choi, A. J. Bandodkar, J. T. Reeder, T. R. Ray, A. Turnquist, S. B. Kim, N. Nyberg, A. Hourlier-Fargette, J. B. Model, A. J. Aranyosi, *ACS sensors* **2019**, *4*, 379.

[39] A. Koh, D. Kang, Y. Xue, S. Lee, R. M. Pielak, J. Kim, T. Hwang, S. Min, A. Banks, P. Bastien, *Science translational medicine* **2016**, *8*, 366ra165.

[40] J. Kim, J. R. Sempionatto, S. Imani, M. C. Hartel, A. Barfidokht, G. Tang, A. S. Campbell, P. P. Mercier, J. Wang, *Advanced Science* **2018**, *5*, 1800880.

[41] S. Emaminejad, W. Gao, E. Wu, Z. A. Davies, H. Y. Y. Nyein, S. Challa, S. P. Ryan, H. M. Fahad, K. Chen, Z. Shahpar, *Proceedings of the National Academy of*

sciences **2017**,*114*, 4625.

[42] P. M. Farrell, T. B. White, C. L. Ren, S. E. Hempstead, F. Accurso, N. Derichs, M. Howenstine, S. A. McColley, M. Rock, M. Rosenfeld, *The Journal of pediatrics* **2017**, *181*, S4.

[43] A. Hauke, P. Simmers, Y. Ojha, B. Cameron, R. Ballweg, T. Zhang, N. Twine, M. Brothers, E. Gomez, J. Heikenfeld, Lab on a Chip 2018, 18, 3750.

[44] J. Kim, I. Jeerapan, S. Imani, T. N. Cho, A. Bandodkar, S. Cinti, P. P. Mercier, J. Wang, *Acs Sensors* **2016**, *1*, 1011.

[45] S. Emaminejad, W. Gao, E. Wu, Z. A. Davies, H. Y. Y. Nyein, S. Challa, S. P. Ryan, H. M. Fahad, K. Chen, Z. Shahpar, *Proceedings of the National Academy of sciences* **2017**, *114*, 4625.

[46] J. R. Sempionatto, A. A. Khorshed, A. Ahmed, A. N. De Loyola e Silva, A. Barfidokht, L. Yin, K. Y. Goud, M. A. Mohamed, E. Bailey, J. May, *ACS sensors* **2020**.

[47] Y. Zhao, B. Wang, H. Hojaiji, Z. Wang, S. Lin, C. Yeung, H. Lin, P. Nguyen, K. Chiu, K. Salahi, *Science advances* **2020**, *6*, eaaz0007.

[48] L. B. Baker, C. T. Ungaro, K. A. Barnes, R. P. Nuccio, A. J. Reimel, J. R. Stofan, Physiological Reports 2014, 2, e12007.

[49] A. Tiwari, H. K. Patra, A. P. Turner, *Advanced Bioelectronic Materials*, John Wiley & Sons, **2015**.

[50] T. Guinovart, G. A. Crespo, F. X. Rius, F. J. Andrade, *Analytica chimica acta* **2014**, *821*, 72.

[51] J. T. Reeder, J. Choi, Y. Xue, P. Gutruf, J. Hanson, M. Liu, T. Ray, A. J. Bandodkar, R. Avila, W. Xia, *Science advances* **2019**, *5*, eaau6356.

[52] M. Parrilla, J. Ferré, T. Guinovart, F. J. Andrade, *Electroanalysis* **2016**, *28*, 1267.

[53] Y. Song, J. Min, Y. Yu, H. Wang, Y. Yang, H. Zhang, W. Gao, *Science advances*

2020, *6*, eaay9842.

[54] M. Parrilla, I. Ortiz-Gomez, R. Canovas, A. Salinas-Castillo, M. Cuartero, G. A. Crespo, *Analytical chemistry* **2019**, *91*, 8644.

[55] M. Bariya, Z. Shahpar, H. Park, J. Sun, Y. Jung, W. Gao, H. Y. Y. Nyein, T. S. Liaw, L.-C. Tai, Q. P. Ngo, *ACS nano* **2018**, *12*, 6978.

[56] M. Parrilla, R. Cánovas, I. Jeerapan, F. J. Andrade, J. Wang, *Advanced healthcare materials* **2016**, *5*, 996.

[57] A. J. Bandodkar, D. Molinnus, O. Mirza, T. Guinovart, J. R. Windmiller, G. Valdés-Ramírez, F. J. Andrade, M. J. Schöning, J. Wang, *Biosensors and bioelectronics* **2014**, *54*, 603.

[58] W. He, C. Wang, H. Wang, M. Jian, W. Lu, X. Liang, X. Zhang, F. Yang, Y. Zhang, *Science advances* **2019**, *5*, eaax0649.

[59] Z. Yuan, L. Hou, M. Bariya, H. Y. Y. Nyein, L.-C. Tai, W. Ji, L. Li, A. Javey, *Lab on a Chip* **2019**, *19*, 3179.

Available at: https://doi.org/10.1002/admt.202000910

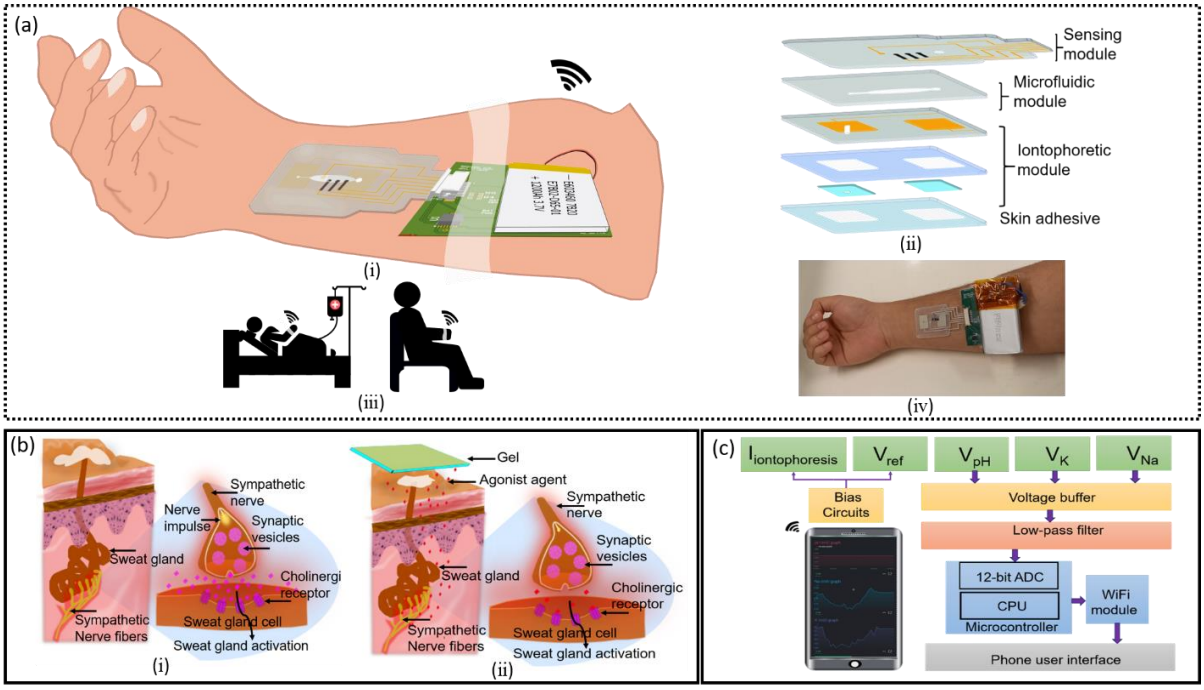

Figure 1. (a) Schematic representation of IIFSP patch attached to the wrist (i), exploded view of the patch illustrating sweat stimulation, transport, and sensing modules (ii), application of

sweat patch for sweat analysis during a stationary condition (iii), and optical image of IIFSP worn on subject wrist (iv). (b) Illustration of sweat induction by natural sweating (i), as compared to iontophoretic process (ii), and (d) block diagram of developed PCB and smartphone interface.

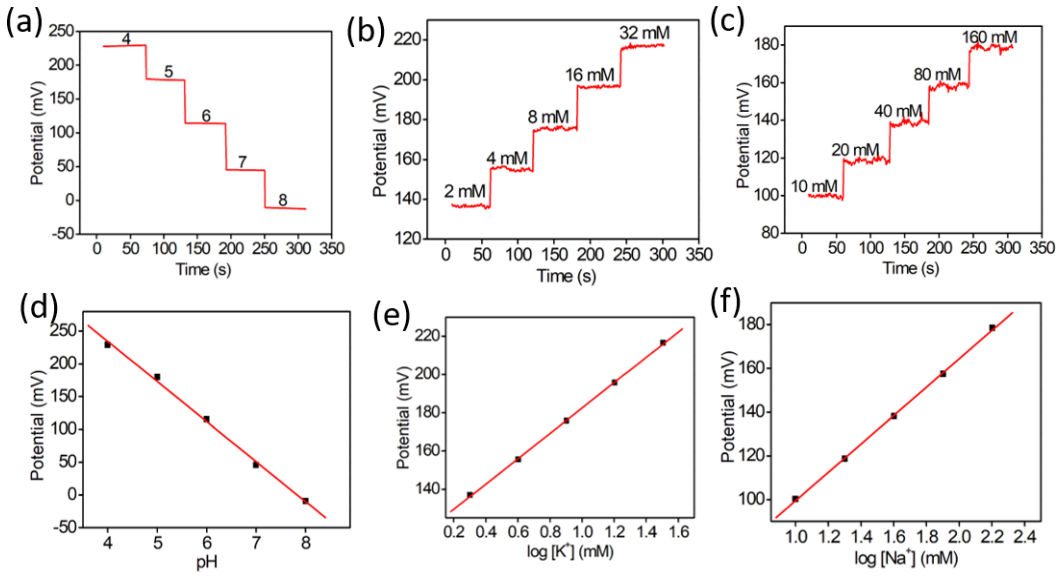

Figure 2. Open circuit potential (OCP) response of (a) H^+ sensor, (b) K^+ sensor, (c) Na^+ sensor, and calibration curve for (d) H^+ sensor, (e) K^+ sensor, (f) Na^+ sensor in their respective ionic solutions.

Available at: https://doi.org/10.1002/admt.202000910

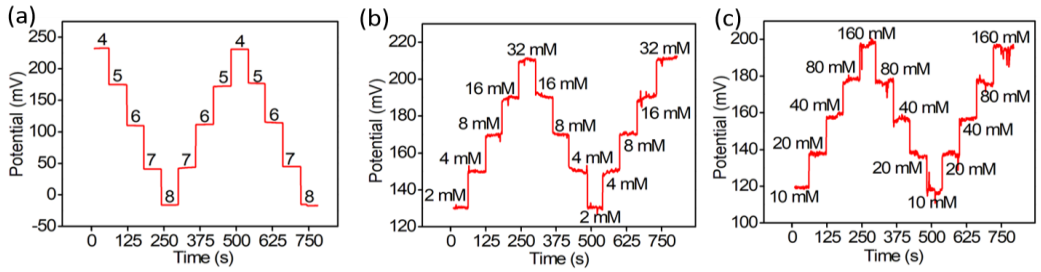

Figure 3. Repeatability of (a) H^+ sensor, (b) K^+ sensor, (c) Na^+ sensor in their respective ionic solutions.

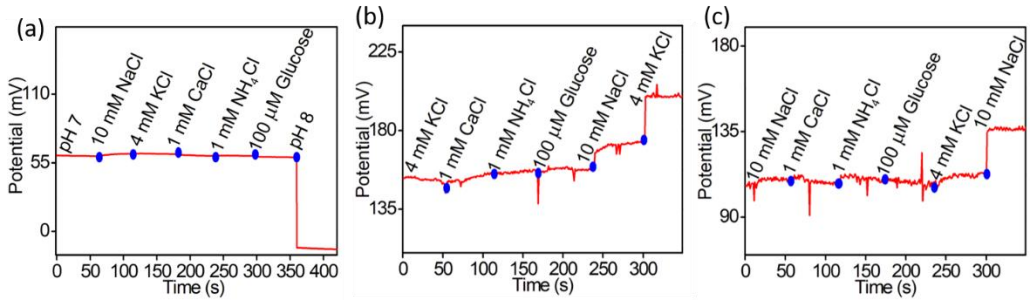

Figure 4. Selectivity evaluation of (a) H^+, (b) K^+, and (c) Na^+ sensors in their respective ionic solutions in the presence of physiologically relevant concentrations of possible interfering ions.

Available at: https://doi.org/10.1002/admt.202000910

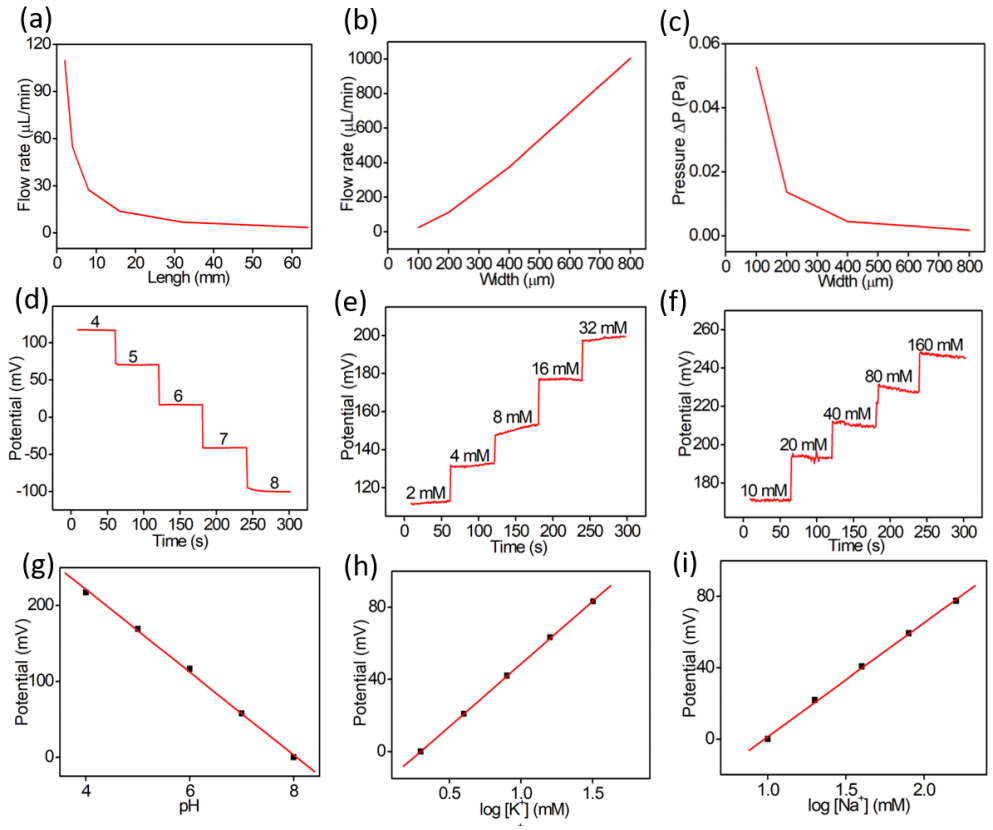

Figure 5. Flow rate dependency optimization on (a) length and (b) width of the microfluidic module, (c) pressure drop dependence on the width of the channel, and responses of (d) pH, (e) K^+, and (f) Na^+ sensors in the artificial sweat through the microfluidic-incorporated device with a constant flow rate of 2 μL/min, and respective baseline-corrected calibration curve for (g) pH, (h) K^+, and (i) Na^+ sensors.

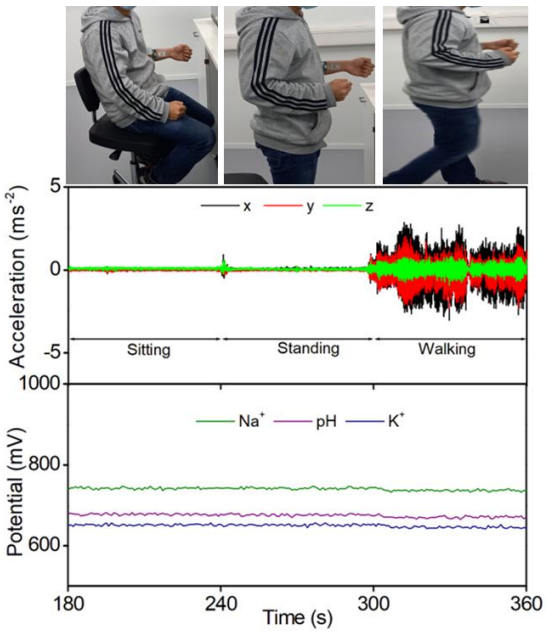

Figure 6.Custom-developed IIFSP for on-body applications. Illustration of stability of Na^+, pH, and K^+ sensors during the sitting, standing, and slow walking activities (the monitored acceleration profile during the activities are depicted in the top).

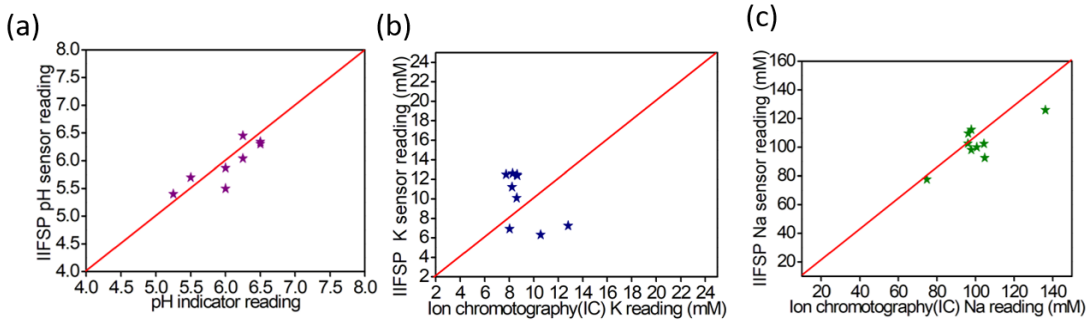

Figure 7. Chart showing correlation between ion chromatography measurements and the developed IIFSP for different sweat samples to validate pH (a), K^+ (b), Na^+ (c) sensors.

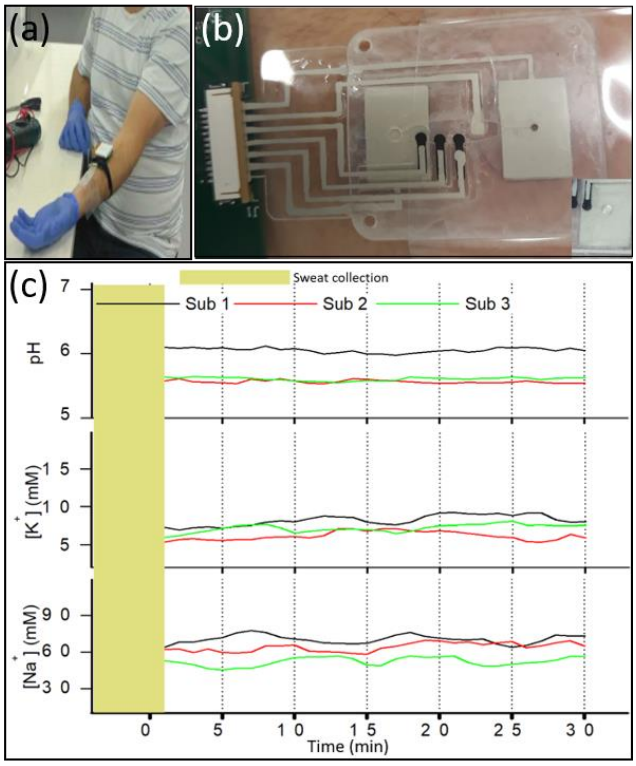

Figure 8. On-body analysis of sweat during stationary conditions. (a) IIFSP is worn on the forearm of a subject for sweat induction, collection, and the data are transmitted to the smartphone-based application for analysis, (b) sweat collection in the IIFSP and inset on the bottom-right corner shows sweat flow at the outlet of the patch (detailed view of each components of IIFSP is shown in Figure S18, Supporting Information), (c) concentration

profiles of H^+, K^+, and Na^+ ions in the sweat of three subjects from IIFSP measurements. The last 30 mins of measurements were recorded after the patch completely filled with sweat and stabilized response from the IIFSP obtained.